Geoscience Frontiers 10 (2019) 2189–2202

HOSTED BY

Contents lists available at ScienceDirect

China University of Geosciences (Beijing)

Geoscience Frontiers

journal homepage: www.elsevier.com/locate/gsf

Research Paper

Continental accretion and incremental deformation in the thermochronologic evolution of the Lesser Caucasus

William Cavazza [a,*], Irene Albino [a], Ghazar Galoyan [b], Massimiliano Zattin [c], Silvia Cattò [a]

[a] Department of Biological, Geological, and Environmental Sciences, University of Bologna, Italy
[b] Institute of Geological Sciences, National Academy of Sciences, Yerevan, Armenia
[c] Department of Geosciences, University of Padua, Italy

ARTICLE INFO

Article history:
Received 25 July 2018
Received in revised form
8 December 2018
Accepted 18 February 2019
Available online 5 April 2019
Handling Editor: Christopher J Spencer

Keywords:
Lesser Caucasus
Low-temperature thermochronology
Apatite fission-track analysis
Structural reactivation
Far-field tectonics

ABSTRACT

Apatite fission-track analysis and thermochronologic statistical modeling of Precambrian–Oligocene plutonic and metamorphic rocks from the Lesser Caucasus resolve two discrete cooling episodes. Cooling occurred during incremental crustal shortening due to obduction and continental accretion along the margins of the northern branch of the Neotethys. (1) The thermochronometric record of a Late Cretaceous (Turonian–Maastrichtian) cooling/exhumation event, coeval to widespread ophiolite obduction, is still present only in a relatively small area of the upper plate of the Amasia-Sevan-Akera (ASA) suture zone, i.e. the suture marking the final closure of the northern Neotethys during the Paleogene. Such area has not been affected by significant later exhumation. (2) Rapid cooling/exhumation occurred in the Early-Middle Miocene in both the lower and upper plates of the ASA suture zone, obscuring previous thermochronologic signatures over most of the study area. Miocene contractional reactivation of the ASA suture zone occurred contemporaneously with the main phase of shortening and exhumation along the Bitlis suture zone marking the closure of the southern branch of the Neotethys and the ensuing Arabia-Eurasia collision. Miocene collisional stress from the Bitlis suture zone was transmitted northward across the Anatolian hinterland, which was left relatively undeformed, and focused along preexisting structural discontinuities such as the eastern Pontides and the ASA suture zone.

1. Introduction

Horizontal compressional stress can travel far from continent-continent collision zones inducing an array of compressional/transpressional structural features such as lithosphere-scale folding, basement upthrusting, and basin inversion both in the foreland and the hinterland (Zoback, 1992; Ziegler et al., 1995, 1998, 2002; Cloetingh et al., 2005; Cowgill et al., 2016). Collision-related stresses can bypass the orogenic wedge and focus along rheological discontinuities at distances in excess of 10^3 km from the collisional front (Ziegler et al., 2002). Strong mechanical coupling between the collisional orogenic wedge and its foreland promotes efficient far-field stress transfer and the ensuing onset and evolution of intra-plate compressional features. Variations in mechanical coupling can be controlled by plate convergence rates and direction, the geometry of the collisional zone, and the rheology and structural fabric of the plates (Cloetingh et al., 1982, 1989; Jolivet et al., 1989; Ziegler, 1993), particularly by upper-plate anisotropy.

The collision between Arabia and Eurasia led to the development of the Bitlis-Zagros orogenic prism and a number of foreland structural features, including (i) the North and East Anatolian Fault systems, (ii) the structural inversion of the Trancaucasian basin(s), (iii) widespread deformation in what is now the Anatolian-Armenian-Iranian plateau, and (iv) faulted anticlines in the flexured Arabian lower plate (Fig. 1). Despite the importance of the event, the timing of collision-related deformation has been long debated, with estimates ranging from Late Cretaceous (Hall, 1976; Berberian and King, 1981; Alavi, 1994), to Late Eocene–Oligocene (35–25 Ma; Jolivet and Faccenna, 2000; Agard et al., 2005; Allen and Amstrong, 2008), to Miocene (Dewey et al., 1986; Yılmaz, 1993; Şengör et al., 2005; Robertson et al., 2007). Recent thermochronologic data have shown that the Bitlis orogenic wedge underwent a significant and discrete mid-Miocene phase of rapid

* Corresponding author. Department of Biological, Geological, and Environmental Sciences, University of Bologna, Piazza di Porta San Donato 1, 40126, Bologna, Italy.
E-mail address: william.cavazza@unibo.it (W. Cavazza).
Peer-review under responsibility of China University of Geosciences (Beijing).

https://doi.org/10.1016/j.gsf.2019.02.007

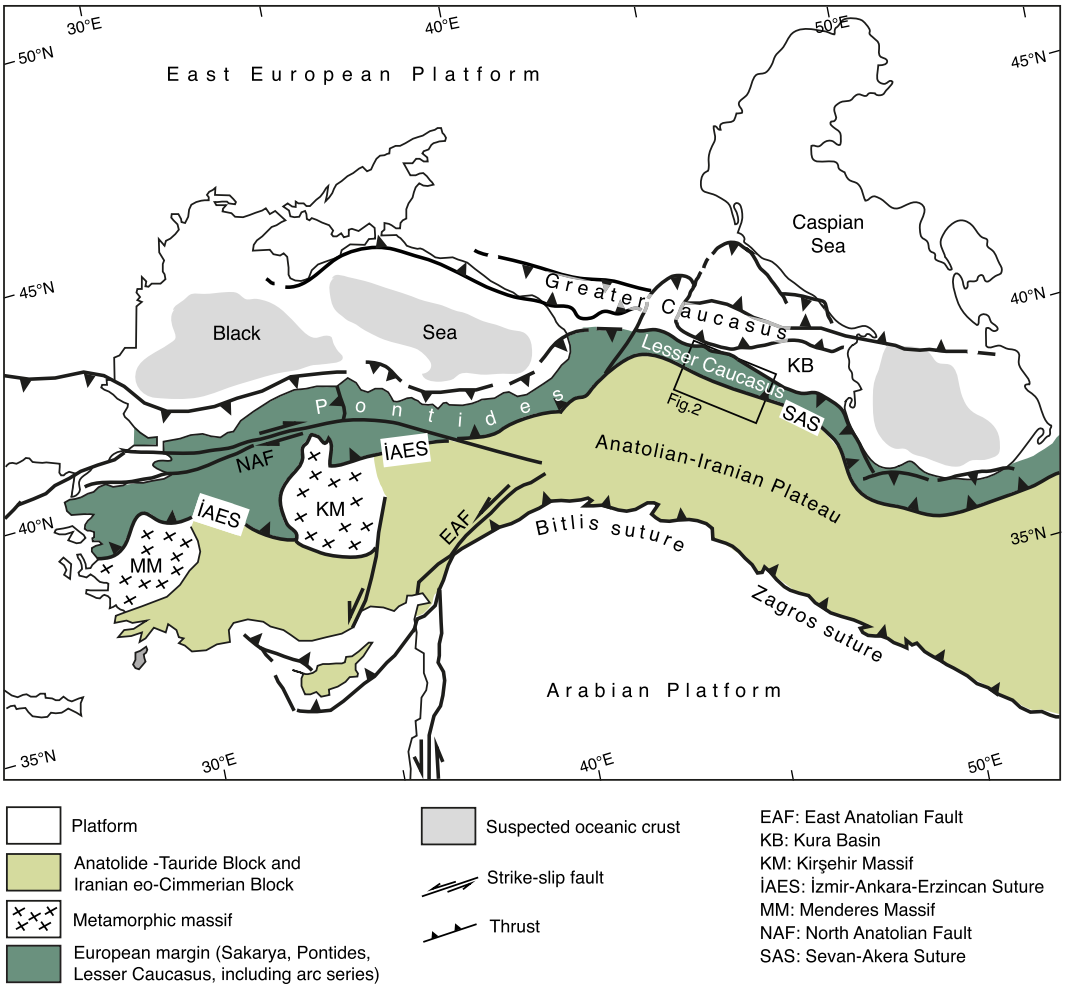

Figure 1. Tectonic sketch map of Asia Minor and the Caucasian region (modified after Sosson et al., 2010). Location of Fig. 2 is shown.

growth by both frontal accretion, as shown by cooling/exhumation of the foreland deposits on both sides of the orogenic prism, and underplating, as shown by cooling/exhumation of the central metamorphic core of the orogenic wedge (Okay et al., 2010; Cavazza et al., 2018). The thermochronologic analysis of the Bitlis orogenic prism does not support the notion of a pre-Miocene collision. Compilation of all geochronometric data available for the entire Bitlis segment of the Arabia-Eurasia collision zone, integrated by stratigraphic and structural relationships, provides a fair reconstruction of the entire time-temperature evolution of the collision zone and point consistently to a Miocene Arabia-Eurasia collision (see discussion in Cavazza et al., 2018). In addition, there is no evidence of a coherent collision-related foreland basin stratigraphy for the Paleogene. If the Arabia-Eurasia collision took place in the Paleogene one would expect the presence of large volumes of orogen-derived sediments on the flexured lower (Arabian) plate, whereas the Paleogene succession south of the Bitlis-Pütürge orogenic prism lacks evidence of synorogenic sedimentation. The development of flexural basins on the lower plate is the hallmark of continental collision and the only record of a crustal section lost to erosion driven by crustal shortening/thickening and subsequent isostatic rebound. The only orogen-derived clastic wedges present on the Arabian plate are Miocene in age wheras the Paleogene section is dominated by laterally extensive shallow-marine carbonates controlled by eustatic sealevel variations and incompatible with active tectonics (e.g. Alsharhan and Nairn, 1997; Yılmaz and Duran, 1997; Jassim and Goff, 2006). The notion of a collision so "soft" as to leave no stratigraphic record cannot be shared. It can be concluded that the Arabia-Eurasia continental collision started in the Miocene.

Low-temperature thermochronological data for the Eurasian foreland north of the Bitlis-Pütürge suture zone suggest that Miocene tectonic stresses related to the Arabian collision were transmitted efficiently over large distances, focusing preferentially at preexisting rheological discontinuities (Albino et al., 2014; Cavazza et al., 2017). Stress concentrated along the marked rheological difference between the polydeformed continental lithosphere of the Eastern Pontides and the relatively pristine quasi-oceanic lithosphere of the eastern Black Sea. Cavazza et al. (2017) showed preliminary data on the northern segment of the Amasia-Sevan-Akera suture zone (Lesser Caucasus) indicating significant mid-Miocene reactivation of this structure. In this paper, we present the first complete low-temperature thermochronological investigation of the entire Lesser Caucasus, concluding that portions of the Lesser Caucasus have preserved the tectonostratigraphic and thermotectonic record of an earlier episode of oceanic obduction and continental accretion, i.e. the result of the Late Cretaceous–Eocene obliteration of the northern Neotethys and the ensuing collision between Eurasia and the Anatolide-Tauride terrane. Other properly oriented segments of the Amasia-Sevan-Akera suture zone were reactivated during the Miocene,

synchronously with maximum mechanical coupling along the Arabia-Eurasia collision front ca. 250 km to the south.

2. Geological setting

The Amasia-Sevan-Akera (ASA) ophiolite belt (Knipper, 1975; Adamia et al., 2011) stretches in a NW–SE direction for about 400 km along the axis of the Lesser Caucasus (Caucasus Minor) (Figs. 2 and 3). The belt is made of outcrops of heavily deformed Middle Jurassic ultrabasic rocks, gabbros, and basalts overlain by pelagic sedimentary deposits. The ophiolite belt is thrust to the southwest and it is floored by a basal tectonic mélange made of greenschist facies metaophiolites and lenses of amphibolite and blueschist (Rolland et al., 2009a, 2010). Scattered outcrops of ophiolites occurring southwest of the ASA belt occur in the Vedi (Sokolov, 1977) and Zangezur (Aslanyan and Satian, 1977; Knipper and Khain, 1980) regions of Armenia, as far as 70 km away from the main suture. These two ophiolite bodies are now considered as *klippen* of the main ASA ophiolite belt (Galoyan, 2008; Sosson et al., 2010) which were obducted southward onto the South Armenian block, the probable eastward continuation of Anatolia (Hässig et al., 2016a, b). The petrochemical characteristics of the ophiolite belt and the associated *klippen* indicate an overall tholeiitic tendency influenced by a subduction component (for a review, see Rolland et al., 2010).

The ASA ophiolite belt separates Variscan terranes of Eurasian affinity to the north from Panafrican terranes of Gondwanian affinity to the south (Rolland et al., 2012, 2016 and refs. therein). From this viewpoint, it plays the same role of the Izmir-Ankara-Erzincan suture of Anatolia of which it can be considered the eastward prolongation (Khain, 1994; Okay and Tüysüz, 1999; Adamia et al., 2011; Hässig et al., 2013b, 2015a, b). The geographic proximity and similarity in the geological units suggest a parallel evolution between northeastern Anatolia and the Lesser Caucasus (Knipper, 1975; Okay and Tüysüz, 1999; Hässig et al., 2013a, b). In the Lesser Caucasus the southwestward obduction of oceanic lithosphere on the Anatolide-Tauride block occurred during the Late Cretaceous at 95–84 Ma (Sokolov, 1977; Knipper and Khain, 1980; Sosson et al., 2010; Hässig et al., 2016a, b). Traditionally, it was thought that the obduction was directly related to continental collision but more recent paleogeographic reconstructions envision an early (Campanian) episode of ophiolite obduction unrelated to collision along the northern continental margin of the Anatolide-Tauride block followed by diachronous collision of irregular continental margins in the Maastrichtian-Ypresian (Stampfli et al., 2001; Cavazza et al., 2004; Barrier and Vrielynck, 2008; Rolland et al., 2009a). During continental collision the Eurasian plate overthrust the ophiolite southward but large outcrops of the obducted ophiolite remain either as isolated *klippen* or reworked mélange.

Subduction of the northern Neotethys underneath the southern European continental margin prior to collision is evidenced by the Somkheto-Karabakh magmatic arc, a thick and mainly calcalkaline magmatic arc and associated volcaniclastic series dated as Bajocian to Santonian (Knipper, 1975; Adamia et al., 1987; Ricou et al., 1986; Sosson et al., 2010; Galoyan et al., 2018). The basement complex of the European margin is mostly Variscan in age and crops out in three main metamorphic salients in Georgian

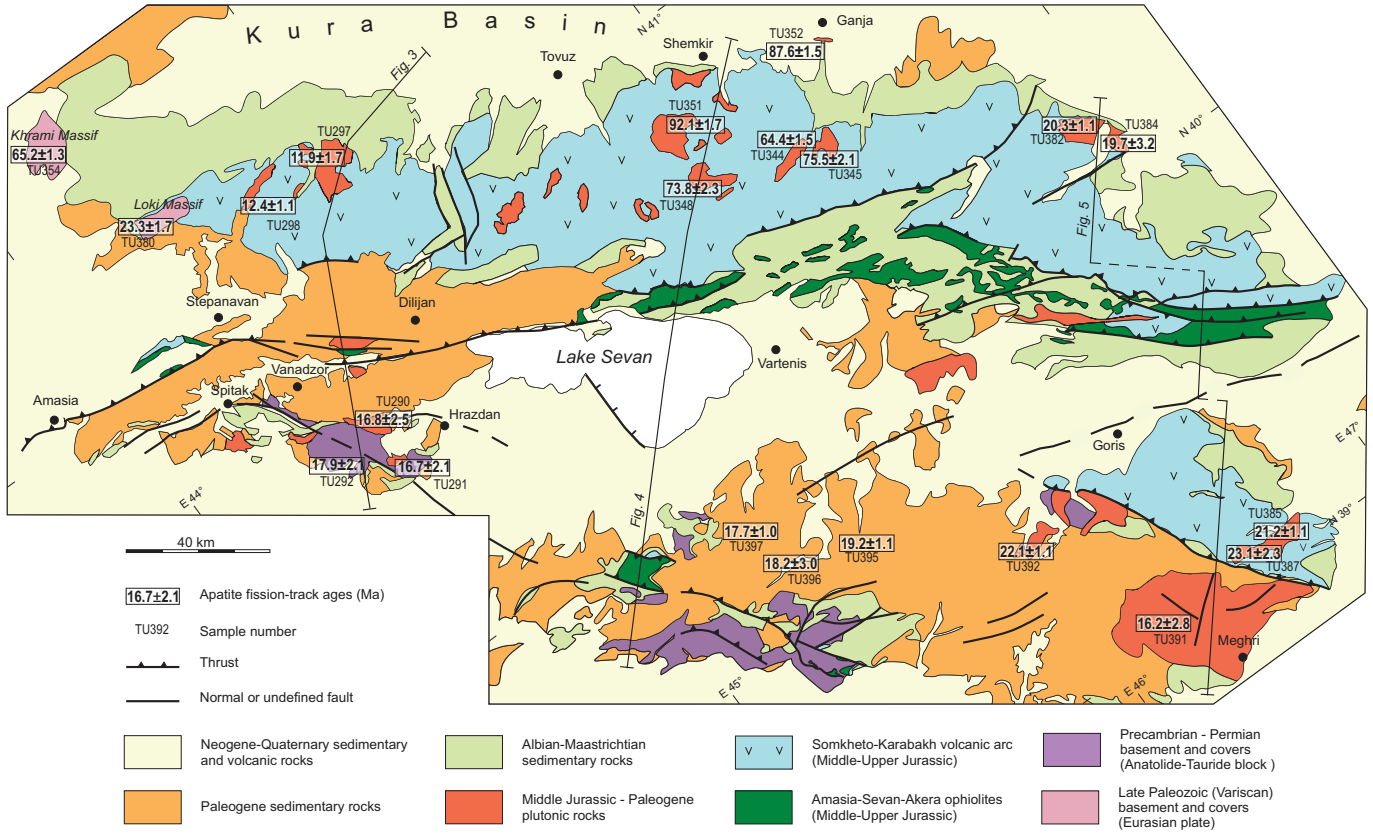

Figure 2. Geological sketch map of the Lesser Caucasus (after Sosson et al., 2010). Apatite fission-track model ages are shown (for analytical details and exact sample locations, see Table 1). Traces of geological cross-sections of Figs. 3–5 are also shown.

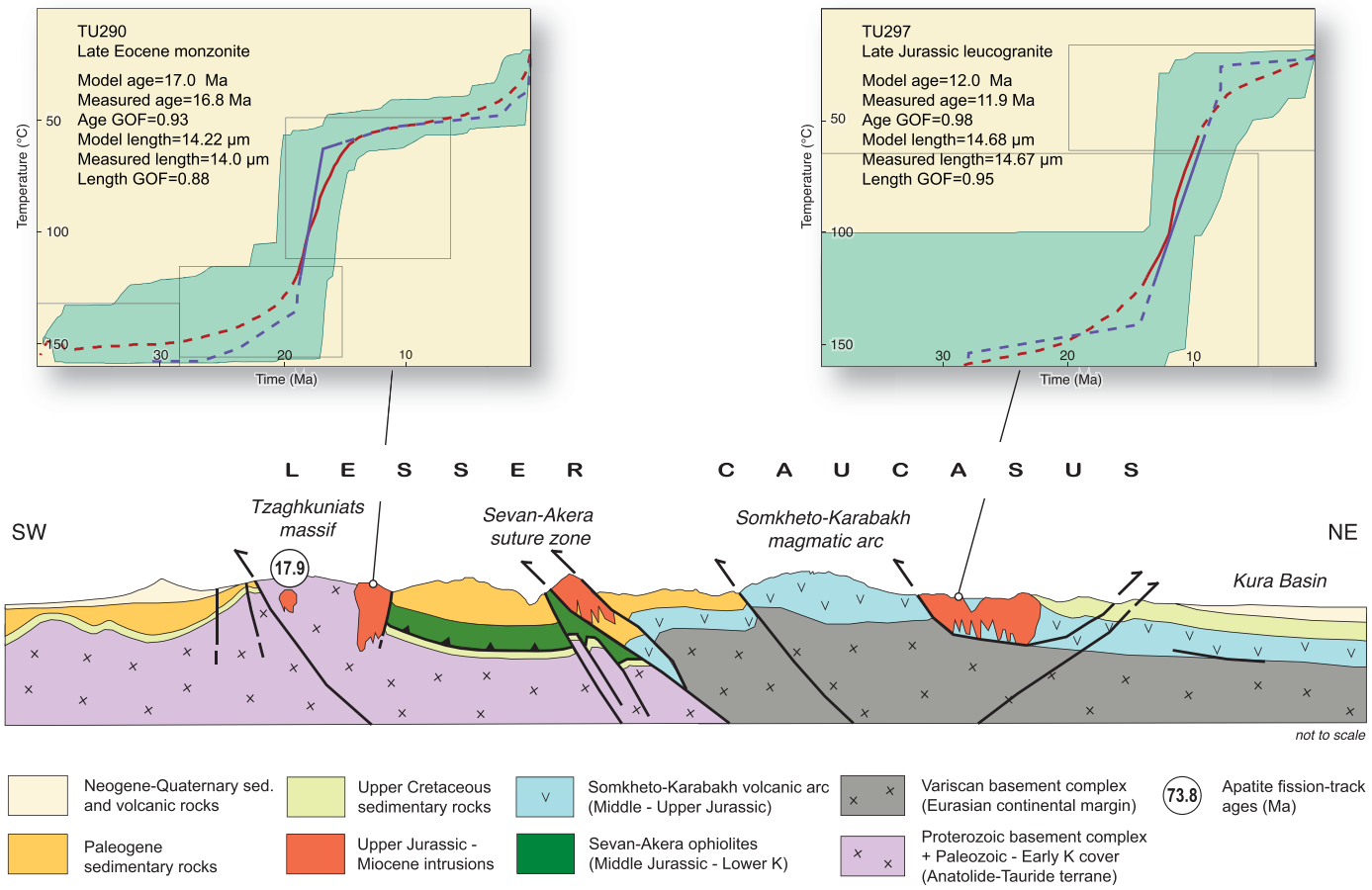

Figure 3. Schematic geological section across the northern Lesser Caucasus (see Fig. 2 for location). Modified after Ministry of Geology USSR (1952a, b). The extent of a large slab of southwestward-obducted ophiolite along the Sevan-Akera suture is inferential. Only the fission-track ages and thermochronologic models closest to the trace of the cross-section are shown; see Fig. 2 and Table 1 for the complete dataset. Time-temperature paths were obtained from integrated inverse modeling of apatite fission-track data from samples TU290 and TU297. Green areas mark envelopes of statistically acceptable fit, and the lines correspond to the most probable thermal histories: red line is the mean of all statistically acceptable paths; blue line is the best-fit T-t path. Parameters related to inverse modeling are reported: GOF, goodness-of-fit gives an indication about the fit between observed and predicted data (values closer to 1 are best).

territory: the Dzirula, Khrami and Loki massifs (Rolland et al., 2011) (Fig. 2). The overlying stratigraphic succession is relatively well exposed along the northeastern part of the Lesser Caucasus and can be summarized as follows (for details, see Sosson et al., 2010). A ca. 3000 m thick Bajocian–Bathonian section dominated by basalts, volcanoclastic turbidites and andesite overlies the Variscan basement, indicating major magmatic activity during the Middle Jurassic. The Late Jurassic succession represents a transgressive trend with conglomerate, mudrock, and reef limestone. The Kimmeridgian features widespread intrusions (granodiorite, gabbro, quartz-diorite, plagiogranite) (Melkonyan, 1989) with a number of associated ore deposits. The Early Cretaceous–early Late Cretaceous units have reduced thickness and comprise a variety of terrestrial and shallow marine environments. Late Turonian or Coniacian formations overlie unconformably the Late Jurassic intrusions and the earlier Cretaceous units. This unconformity is a supraregional feature and can be traced southeastward along the northeastern flank of Caucasus Minor to Karabakh, where it covers a relatively short time span within the Turonian (Abdullayev, 1963). The Senonian succession comprises pillow- and massive-basalt lava flows. Thus the magmatic arc was still active during this period of time along this part of the Eurasian margin. The end of magmatic activity occurred in Campanian to Maastrichtian times.

The terrane directly south of the ASA suture zone has been termed South Armenia Block or, alternatively, Daralagez terrane (Knipper, 1975; Knipper and Khain, 1980; Zonenshein et al., 1990) and is considered as the eastern continuation of the Anatolide-Tauride terrane of Turkey (Knipper, 1975; Okay and Tüysüz, 1999). Its basement, well exposed in the Tsaghkuniats massif northeast of Yerevan (Fig. 2), is made of Proterozoic metamorphic rocks (gneiss, micaschist) intruded by leucogranite. This basement underwent Late Jurassic (syn-subduction) MP-MT metamorphism at 160–150 Ma followed by LP-HT overprint (and doming) at 130–120 Ma (Hässig et al., 2015b). The overlying incomplete Paleozoic sedimentary succession crops out in southwestern Armenia and Nakhijevan. It is made of a >1500 m thick section of Late Devonian (Frasnian–Famennian) sandstone/mudrock and Carboniferous reefal limestone, disconformably overlain by Permian–Early Triassic carbonates evolving upsection into Middle-Late Triassic siliciclastic sandstone and mudrock (Arakelyan, 1964). The Jurassic system is cropping out only at a distance from the ASA suture zone in northern Iran and Nakhijevan, where carbonate platformal facies are predominant. Thick Early Cretaceous reef limestone overlies unconformably all previous formations and is overlain by a Late Cenomanian–Turonian flysch (Danelian et al., 2014) and by Late Coniacian–Santonian olistostrome bodies (Sokolov, 1977; Sosson et al., 2010) made of

Table 1
Results of apatite fission-track analyses (see Fig. 2 for location of samples).

Sample	Rock type	Location	Age	Elevation (m)	UTM coordinates (38T)	No. crystals	Spontaneous		Induced		$P(\chi)^2$	Dosimeter		Age (Ma) ± 1s	MCTL (mm) ± standard error	Standard deviation	No. tracks measured
							ρ_s	N_s	ρ_i	N_i		ρ_d	N_d				
TU290[a]	Monzonite	Aghavnadzor	Late Eocene	1846	475087, 4492519	17	1.75	57	17.32	559	99.43	9.8	4798	16.8 ± 2.5	14.50 ± 0.09	0.70	55
TU291[a]	Orthogneiss	Bjni	Precambrian	1788	469751, 4480111	20	1.91	80	18.45	773	80.92	9.6	4798	16.7 ± 2.1	12.70 ± 0.32	1.02	10
TU292[a]	Tonalite	NW of Arzakan	Late Jurassic	1923	463243, 4484734	20	2.05	101	18.30	898	95.68	9.5	4798	17.9 ± 2.1	13.45 ± 0.40	1.40	12
TU297[a]	Leucogranite	Mets Ayrum	Late Jurassic	665	484745, 4558283	21	1.53	59	18.83	722	98.77	9.7	4798	11.9 ± 1.7	14.58 ± 0.11	0.80	50
TU298[a]	Plagiogranite	E of Alaverdi	Middle Jurassic	661	475628, 4551062	20	2.26	179	16.83	1134	100.00	9.8	4798	12.4 ± 1.1	-	-	-
TU344[a]	Granodiorite	Dashkesan pluton	Late Jurassic	1438	591398, 4483554	20	4.73	257	11.90	648	100.00	11.0	4231	64.4 ± 1.5	-	-	-
TU345[a]	Granodiorite	Dashkesan pluton	Late Jurassic	1545	592153, 4482654	20	5.01	276	12.92	713	98.20	11.2	4578	75.5 ± 2.1	-	-	-
TU348[a]	Diorite	Gedabey mine	Late Jurassic	1539	567870, 4492625	18	5.09	281	12.89	711	100.00	11.4	4356	73.8 ± 2.3	13.65 ± 0.18	0.84	21
TU351[a]	Granite	Ertepe pluton	Middle Jurassic	1677	575265, 4498811	21	8.29	442	17.92	955	89.98	12.0	4798	92.1 ± 1.7	13.42 ± 0.27	1.55	31
TU352[a]	Granodiorite	Uchtepe pluton	Early Cretaceous	507	612216, 4500380	20	8.43	456	17.64	940	87.68	13.0	4678	87.6 ± 1.5	-	-	-
TU354	Granite	Khrami Massif	Late Paleozoic	1524	426185, 4599082	21	3.40	175	10.86	540	99.83	9.8	4491	65.2 ± 1.3	-	-	-
TU380	Granite	Berdadzor pluton	Middle Jurassic	1523	635850, 4393421	16	1.79	62	20.20	702	90.14	12.0	4496	23.3 ± 1.7	-	-	-
TU382	Tonalite	Mehmana pluton	Late Jurassic	713	650829, 4443990	21	2.85	180	35.32	2226	89.95	13.0	4197	20.3 ± 1.1	-	-	-
TU384	Granodiorite	Mehmana pluton	Late Jurassic	605	656216, 4438175	20	2.73	169	39.20	1979	97.31	12.0	4273	19.7 ± 3.2	-	-	-
TU385	Tonalite	Tsav pluton	Late Jurassic–Early Cretaceous	1238	627336, 4329451	20	1.65	184	28.71	2078	90.21	9.9	4790	21.2 ± 1.1	-	-	-
TU387	Diorite	Tsav pluton	Late Jurassic–Early Cretaceous	1069	626859, 4323628	23	2.66	133	18.60	933	95.21	10.0	4793	23.1 ± 2.3	-	-	-
TU391	Granite	Meghri pluton	Early Miocene	2153	601645, 4327242	16	3.02	151	24.22	1989	99.24	11.2	4692	16.2 ± 2.8	13.30 ± 0.16	1.23	57
TU392	Granodiorite	Sisian stocks	Middle Eocene	1783	588031, 4362302	25	4.82	374	34.70	2696	80.81	10.0	4599	22.1 ± 1.1	-	-	-
TU395	Granodiorite	Jermuk/Vaik stocks	Late Oligocene–Early Miocene	1320	544108, 4393482	17	2.73	170	40.77	2345	89.91	10.0	4696	19.2 ± 1.1	12.62 ± 0.11	0.85	51
TU396	Granodiorite	Yeghegnadzor	Late Oligocene–Early Miocene	1113	528198, 4398800	25	2.61	160	22.26	1364	99.94	10.0	4992	18.2 ± 3.0	-	-	-
TU397	Diorite	Salli	Late Eocene	1580	523785, 4413779	18	2.29	107	26.51	1213	91.12	12.0	4875	17.7 ± 1.0	-	-	-

MCTL: mean confined track length. Central ages calculated using dosimeter glass CN5 and z-CN5 = 336.34 ± 16.24 Ma (analyst I. Albino). ρ_s: spontaneous track densities ($\times 10^5$ cm^{-2}) measured in internal mineral surfaces; N_s: total number of spontaneous tracks; ρ_i and ρ_d: induced and dosimeter track densities ($\times 10^6$ cm^{-2}) on external mica detectors ($g = 0.5$); N_i and N_d: total numbers of tracks; $P(\chi^2)$: probability of obtaining χ^2-value for n degrees of freedom (where n = number of crystals-1); a probability >5% is indicative of an homogenous population.

[a] Ages from Cavazza et al. (2017) (analyst I. Albino).

ophiolitic blocks in a pelitic matrix. These olistostromes are considered as forerunners of the widespread ophiolite obduction episode across the northern margin of the Anatolide-Tauride-Armenia terrane during the latest Cretaceous (e.g. Hassig et al., 2013a, b). The onset of collision and limited continental subduction of the Anatolide-Tauride-Armenia terrane below the Pontides Eurasian margin in the Lesser Caucasus is dated as Paleocene (Rolland et al., 2009a; Sosson et al., 2010; Rolland et al., 2012). This process occurred around 20 Ma later than southward ophiolite obduction (Late Coniacian–Santonian, 88–83 Ma) and led to the uplift of the Sevan–Akera suture zone, its folding, erosion and to the transfer of detritus in a flexural basin in front of the belt, above the obduction structures. Throughout the Paleocene and the Early-Middle Eocene a flexural basin covered the obducted ophiolite and related structures, and was progressively deformed along thrusts in its internal (northeastern) sector. It was generally considered that the Miocene marked a transition to mostly strike-slip deformation in the region (e.g. Avagyan et al., 2015) but preliminary thermochronologic data has proven a considerable component of dip-slip movements during this epoch along properly oriented segments of the Sevan-Akera suture zone, both in the lower and upper plates (Cavazza et al., 2017).

3. Analytical methods and samples

3.1. Apatite fission-track analysis and modeling

Fission tracks are linear radiation damages within the crystal lattice, caused by nuclear fission of radioactive isotope ^{238}U, that can be etched and counted under an optical microscope. Concurrently, neutron irradiation is used to induce the decay of ^{235}U, generating radiation damages on the surface of an external detector. Grain-by-grain determination of both spontaneous and induced fission-track densities yields a single-grain age representing the cooling of the grain below a closure temperature of ~100 °C. Fission-track dating is a useful tool to unravel the cooling histories experienced by rocks in the upper crustal levels and to give a measure of their exhumation (for a review of the method, see Donelick et al., 2005). Fission tracks in apatites all have the same initial length of about 16 μm (e.g. Ketcham et al., 1999) but anneal at rates proportional to temperatures, starting at about 60 °C. Over geological time periods, partial annealing of fission tracks occurs at temperatures between about 60 °C and 125 °C (i.e. the Partial-Annealing Zone: PAZ; Gleadow and Fitzgerald, 1987). Because tracks shorten in relation to the degree and duration of heating, the measurement of fission-track lengths gives information about the thermal evolution in the PAZ temperature range. A quantitative evaluation of the thermal history can be carried out through modeling procedures, which find a range of cooling paths compatible with the apatite fission-track (AFT) data (Ketcham, 2005). In this work, inverse modeling of track length data was performed using the HeFTy program (Ehlers et al., 2005), which generates the possible T–t paths by a Monte Carlo algorithm. Predicted AFT data were calculated according to the Ketcham et al. (2007) annealing model for fission tracks revealed by etching. D_{par} values (i.e. the etch pit length) were used to define the annealing kinetic parameters of the grains and the original track length.

3.2. Sampling strategy and sample preparation

Forty-one samples were taken on both sides of the Sevan-Akera suture zone, covering the length of the Lesser Caucasus from the Khrami Massif to the northwest to the southern end of the mostly Jurassic Somkheto-Karabakh magmatic arc to the southeast (Fig. 2). Most samples are from plutonic and metamorphic rocks ranging in age from Precambrian to Jurassic. Younger Oligo-Miocene intrusives from the Armenian highlands were also sampled. Apatite grains were concentrated by crushing and sieving, followed by hydrodynamic, magnetic, and heavy-liquid separations. Apatites were embedded in epoxy resin, polished in order to expose the internal surfaces within the grains, and the spontaneous FT were revealed by etching with 5 N HNO_3 at 20 °C for 20 s. The mounts were then coupled with a low-uranium fission-track-free muscovite mica sheet (external detector method) and sent for irradiation with thermal neutrons (see Donelick et al., 2005, for details) at the Radiation Center of Oregon State University. Nominal fluence of 9×10^{15} n cm^{-2} was monitored with a CN5 uranium-doped silicate glass dosimeter. Induced fission tracks were revealed by etching of the mica sheets in 40% HF for 45 min at 20 °C. Spontaneous and induced fission tracks were counted under an optical microscope at ×1250 magnification, using an automatic stage and a digitizing tablet.

Twenty-one samples of the original set yielded apatites suitable for dating (Table 1). Central ages were calculated with the zeta calibration approach (Hurford and Green, 1983), using Durango (31.3 ± 0.3 Ma) and Fish Canyon Tuff (27.8 ± 0.2 Ma) age standards within grains exposing *c*-axis-parallel crystallographic planes. Track-length distributions were calculated by measuring horizontal confined tracks together with the angle between the track and the *c*-axis. Confined tracks constitute a small part of the FT populations, therefore additional concentrates were mounted, polished and etched for the analysis. Ultimately, six samples contained a statistically significant number of confined tracks. All available geological constraints (intrusion ages, depositional ages, and stratigraphic relationships) were incorporated into the modeling. A first batch of thousands simulations was performed with very large time-temperature constraints. Once a broad range of possible solutions was achieved, the program was forced to work on more restricted time-temperature region (boxes in Figs. 3–5). The distribution of fission-track lengths and geological information support a general picture of simple cooling paths, without relevant post-exhumation burial and additional cooling events. The modeled cooling paths thus provide important constraints on the cooling/exhumation chronology of the study area.

4. Analytical results

Table 1 and Fig. 2 provide a summary of the AFT data. Central ages cluster into two distinct groups. The older age cluster ranges from 92.1 ± 1.7 Ma to 64.4.7 ± 1.5 Ma (Late Cretaceous). The younger age cluster range from 23.3 ± 1.7 Ma to 11.9 ± 1.7 Ma (Early Middle Miocene). All the samples passed the χ^2 test indicating a single population of grains and do not show any correlation between age and elevation. The two age groups show a well defined geographic position, with the older age samples clustering in the hanging wall of ASA suture zone in the central portion of the Somkheto-Karabakh magmatic arc (Fig. 2).

AFT central ages provide an average indication of how the samples cooled across the partial annealing zone (PAZ) of apatite (ca. 60–120 °C) but can be somewhat misleading if the sample resided within the PAZ for a long time. More precise t-T paths can be obtained through statistical modeling of fission-track length distributions. Following are the results of thermochronometric modeling of six samples containing a statistically significant number of confined tracks. We will describe first the AFT analytical results obtained from the samples taken along the European margin (i.e. northeast of the ASA suture zone) and then those from the samples taken along the Anatolide-Tauride-

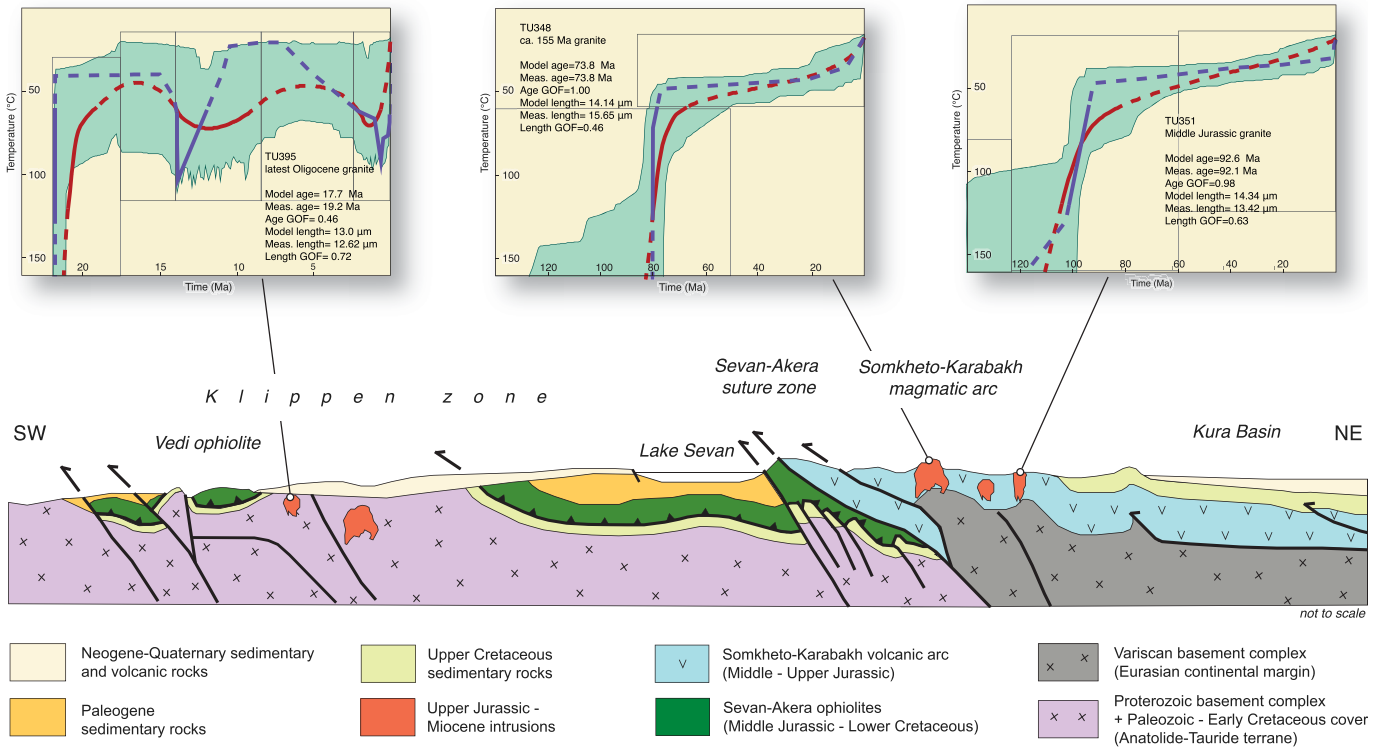

Figure 4. Schematic geological section across the central Lesser Caucasus (see Fig. 2 for location). Modified after Sosson et al. (2010). The section emphasizes the structural pattern produced by shortening during continental collision; the effects of late-stage strike-slip tectonics are largely ignored. Only the fission-track ages closest to the traces of geological cross-sections are shown; see Fig. 2 for the complete dataset. Time-temperature paths were obtained from integrated inverse modeling of apatite fission-track data from samples TU395, TU348 and TU351. Green areas mark envelopes of statistically acceptable fit, and the lines correspond to the most probable thermal histories: red line is the mean of all statistically acceptable paths; blue line is the best-fit T-t path. Parameters related to inverse modeling are reported: GOF, goodness-of-fit gives an indication about the fit between observed and predicted data (values closer to 1 are best).

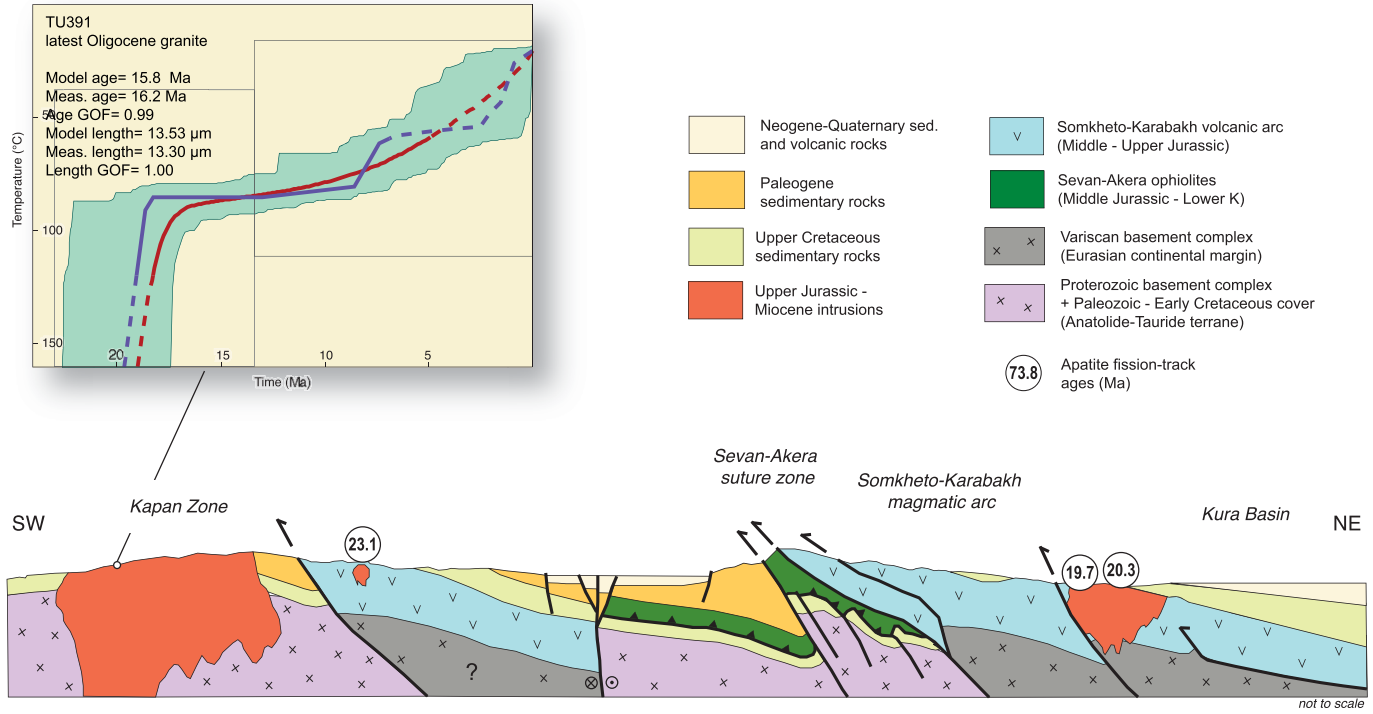

Figure 5. Schematic geological section across the southern Lesser Caucasus (see Fig. 2 for location). Modified after Ministry of Geology USSR (1952c,d, 1971). Interpretation of this cross-section subscribes to the notion that the Kapan Zone represents a section of the Somkheto-Karabakh magmatic arc displaced by large-scale dextral strike-slip. Only the fission-track ages closest to the traces of geological cross-sections are shown; see Fig. 2 for the complete dataset. Time-temperature paths were obtained from integrated inverse modeling of apatite fission-track data from samples TU391. Green areas mark envelopes of statistically acceptable fit, and the lines correspond to the most probable thermal histories: red line is the mean of all statistically acceptable paths; blue line is the best-fit T-t path. Parameters related to inverse modeling are reported: GOF, goodness-of-fit gives an indication about the fit between observed and predicted data (values closer to 1 are best).

Armenian margin. Results of the statistical forward modeling are shown in Figs. 3–5.

4.1. AFT results from the European margin

Sample TU348 is a Late Jurassic diorite dike intruding a granodiorite pluton in the central portion of the Somkheto-Karabakh magmatic arc (Gedabey mine) (Figs. 2 and 4, Table 1). Track-length frequency distribution is platykurtic (Fig. 6); inverse modeling indicates very rapid cooling across the apatite PAZ between 80 Ma and 77 Ma (Campanian).

Sample TU351 is a Middle Jurassic granite from the Ertepe pluton of the central Somkheto-Karabakh magmatic arc (Figs. 2 and 4; Table 1). It yielded a tight cluster of single-grain ages (98–85 Ma), a central age of 92.1 ± 1.7 Ma, a leptokurtic track-length distribution with a single peak, and a relatively short mean track length of 12.16 ± 1.13 μm (Fig. 6). The overall shape of the reconstructed time-temperature path of this sample is similar to the one of sample TU348 from the same region (Fig. 4) despite an older AFT central age.

Three other samples from the central Somkheto-Karabakh magmatic arc were analyzed but did not yield enough confined tracks for a statistically robust inverse modeling. Two granodiorite samples (TU344 and TU345) from the Late Jurassic Dashkesan pluton yielded central ages of 64.4 ± 1.5 Ma and 75.5 ± 2.1 Ma, respectively (Fig. 2; Table 1). The third sample (TU352) was taken from the Early Cretaceous Uchtepe pluton and provided a central age of 87.6 ± 1.5 Ma. Another latest Cretaceous AFT central age came from a Late Paleozoic granitic sample (TU354) from the Khrami Massif of southern Georgia, a Variscan metamorphic salient which underwent some reheating during the Mesozoic (Rolland et al., 2011).

Sample TU297 is a leucogranite from a Late Jurassic granitic-tonalitic body intruding the volcanics/volcaniclastics of the northern Somkheto-Karabakh magmatic arc (Table 1; Fig. 2). The geological setting of this sample is identical to those of samples from the central portion of the arc (see above) but its low-temperature thermochronological evolution (Fig. 3) indicates a discrete, much younger episode of cooling at about 12 Ma (Middle Miocene). Two other samples from the northern Somkheto-Karabakh magmatic arc were analyzed and also yielded Miocene central ages: TU298 (Middle Jurassic plagiogranite from the Alaverdi district; Galoyan et al., 2018; AFT central age 12.4 ± 1.1 Ma) and TU380 (Middle Jurassic granite from the Berdadzor pluton; Galoyan et al., 2018; AFT central age 23.3 ± 1.7 Ma) (Fig. 2). Both samples did not contain enough confined tracks for inverse statistical modeling.

Two samples from the Late Jurassic Mehmana pluton in the southern part of the Somkheto-Karabakh magmatic arc yielded again consistent Miocene AFT central ages. Sample TU382 (tonalite from the Kashen mine) provided an age of 20.3 ± 1.1 Ma. Sample TU384 (coarse-grained tonalite) provided an age of 19.7 ± 3.2 Ma (Table 1; Figs. 2 and 4).

Two samples (TU385 tonalite, TU387 diorite) from the Tsav pluton (Upper Cretaceous; Melkonyan et al., 2016) of the Kapan zone yielded Early Miocene apatite fission-track ages of 21.2 ± 1.1 Ma and 23.1 ± 2.3 Ma, respectively (Fig. 2).

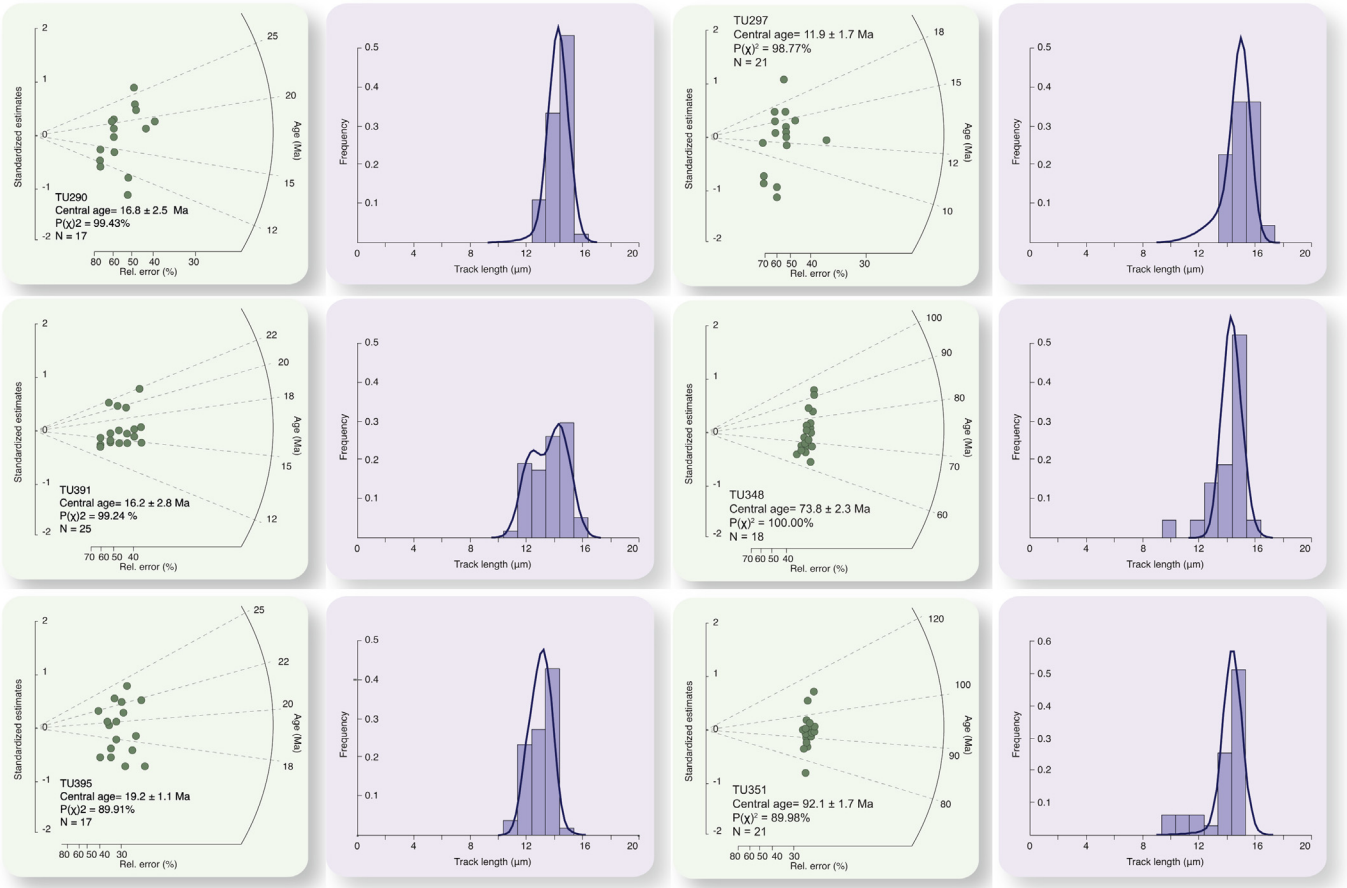

Figure 6. Radial plots of single-grain apatite fission-track ages and histograms showing the confined-track length distributions of apatite grains for the six samples employed for statistical modeling. For analytical details on AFT ages reported in the figure, see Table 1.

4.2. AFT results from the Anatolide-Tauride-Armenian margin

Irrespective of their age (Precambrian to Miocene) and lithology (from orthogneiss to granitoid rocks) all samples from the Anatolide margin yielded coherent Early Miocene apatite fission-track central ages, ranging from 22.1 ± 1.1 Ma to 16.2 ± 2.8 Ma (Fig. 2). Three samples were taken from the crystalline rocks of the Tzaghuniats Massif. Sample TU290 is from the Aghavnadzor intrusion, an Upper Eocene monzonite/monzodiorite body intruding the Proterozoic basement complex of the massif (Table 1; Fig. 2). It yielded a tight cluster of single-grain ages (25–12 Ma), a central age of 16.8 ± 2.5 Ma, and a leptokurtic track-length distribution with a single peak and relatively long mean track length of 14.50 ± 0.14 μm (Fig. 6). The best-fit t-T path shows fast cooling through the PAZ between ca. 19 Ma and 16 Ma (Fig. 4). Both samples TU291 (Precambrian orthogenesiss from the Bjni Massif) and TU292 (Late Jurassic tonalite from Aghveran Massif) did not contain enough confined tracks for inverse modeling but yielded quite consistent Burdigalian (late Early Miocene) FT central ages.

Sample TU391 (porphyritic granite from the northern Meghri-Ordubad pluton in southernmost Armenia) was taken from a pluton which yielded a magmatic age of 22 Ma (earliest Miocene; U–Pb on zircons; Moritz et al., 2016; see also Rezeau et al., 2016, 2017). The AFT central age of this sample is 16.2 ± 2.8 Ma (Table 1) thus implying that cooling to temperatures within the range of the apatite PAZ occurred soon after its emplacement. Inverse modeling (Fig. 5) shows a long residence time within the PAZ and the overall t-T can be interpreted as the result of emplacement at shallow crustal levels (2–3 km).

Sample TU395 is from a Late Oligocene–Early Miocene dike associated with the Vayk intrusion and cutting the thick Middle Eocene volcano-sedimentary succession of the Vayots Dzor province of Armenia. It yielded a tight cluster of single-grain ages (24–17 Ma), a central age of 19.2 ± 1.1 Ma, and a moderately platykurtic track-length distribution with a single peak and a short mean track length of 12.62 ± 0.11 μm (Fig. 6). Overall, this intrusion shows a cooling history very similar to that of TU391, i.e. magmatic cooling followed by a relatively long residence time (from ca. 20 to 2 Ma) within the temperature range of the PAZ (Fig. 4). This dike was emplaced at shallow crustal levels as shown also by the unmetamorphosed Eocene succession nearby. Residence within the PAZ was somehow complicated by two minor heating episodes at about 16–12 Ma and 5–2 Ma. Within the same region, two additional samples (TU396 Late Oligocene–Early Miocene granosyenite; TU397 Late Eocene diorite) did not contain enough confined fission track for inverse modeling but yielded coherent Early Miocene central ages of 18.2 ± 3.0 Ma and 17.7 ± 1.0 Ma, respectively (Fig. 2, Table 1).

A granodiorite sample (TU392) from the Sisian stocks of southern Armenia (Fig. 2) yielded an AFT central age of 22.1 ± 1.1 Ma (Table 1).

5. Discussion

The correlation between low-temperature thermochronometric data and specific geological structures is a difficult task requiring a thorough understanding of the structural setting of the study area. Despite the excellent work done on the Lesser Caucasus, a combination of geological complexity and political fragmentation has hampered a satisfactory understanding of the structural framework of this geological province. From this viewpoint, the cross-sections of Figs. 3–5 ought to be considered rough, tentative depictions of a complex geological structure resulting from incremental deformation and contrasting structural styles. A more comprehensive geological cross-section crossing both the Greater and the Lesser Caucasus is provided by Sosson et al. (2016) (Fig. 2). This paper presents the first low-temperature thermochronometric dataset for the Lesser Caucasus; such dataset is relevant for any future structural interpretation of the region as it provides compelling constraints on its geological evolution. Based on the existing literature and our own observations, following is an attempt at interpreting our dataset within the geological context of the Lesser Caucasus and the surrounding regions.

The AFT thermochronometric dataset presented here documents two distinct episodes of cooling/exhumation in the Lesser Caucasus: during the Late Cretaceous and in Early-Middle Miocene times. These two cooling events can be correlated to the stratigraphic and structural record of the study area and the adjoining regions, as described in the available literature. For example, all along the northeastern flank of the Lesser Caucasus a widespread Turonian unconformity separates either the Middle-Late Jurassic Somkheto-Karabakh magmatic arc (or Early Cretaceous shallow marine sedimentary rocks) from the overlying latest Turonian–Coniacian sedimentary formations (Sosson et al., 2010). The age of such unconformity is an agreement with our Turonian AFT ages (92–88 Ma) in the eastern portion of the Somkheto-Karabakh magmatic arc of northern Azerbaijan west of the city of Ganja (Fig. 2). Portions of the eastern Somkheto-Karabakh magmatic arc were thus exhumed in pre-Coniacian times (see also the modeling of sample TU351 in Fig. 4), concomitant with the southwestward obduction of the Sevan-Akera ophiolites on the Anatolide-Tauride terrane (88–87 Ma; Rolland et al., 2009a, 2010; Sosson et al., 2010; Hässig et al., 2016a, b). Our data show that in the western part of the magmatic arc at the latitude of Ganja the AFT record of the obduction was overprinted by the exhumation of a new apatite partial annealing zone at 75–64 Ma (Late Campanian–Early Danian) (Table 1; Figs. 2 and 4; see also sample TU348 in Fig. 4) during final oceanic closure (74–71 Ma; Rolland et al., 2010; Galoyan et al., 2009; Sosson et al., 2010; Galoyan et al., 2013) and the ensuing continental indentation, lithospheric coupling, and thrusting. Alternatively, one might envision the Cretaceous AFT age pattern found in the southeastern portion of the study area as the result of a single, prolonged exhumation episode.

Late Cretaceous ophiolite obduction along the Anatolide-Tauride-Armenian (and Arabian) northern continental margin has been described from western Anatolia to Oman (e.g. Robertson, 2002; Okay et al., 2010). Such discrete and important episode of ophiolite obduction had significant tectonic effects, including the development of structural relief, lithospheric flexure, and creation of accommodation space for sedimentation. Crustal shortening might have also played an important role during obduction as recent studies in eastern Anatolia (Topuz et al., 2017; Cavazza et al., 2018) point to a coherent metamorphic event across the entire area comprised between the Erzincan-Sevan suture to the north and the Bitlis-Zagros suture to the south. Late Cretaceous metamorphism is coeval with massive southward ophiolite obduction from the northern branch of the Neotethys onto the Anatolide-Tauride terrane (Stampfli and Hochard, 2009; Hässig et al., 2016a, b).

Coherent Neogene AFT ages characterize all other portions of the study area on both sides of the Amasia-Sevan-Akera suture zone (Fig. 2), with central ages ranging from 23.3 Ma to 11.9 Ma (Early-Middle Miocene) (Table 1). Correlation between the thermochronometric data presented here and the activity of specific geological structures of the Lesser Caucasus would require a detailed structural analysis and goes beyond the scope of this work. From a general viewpoint, paleomagnetic data, although not conclusive, indicate that about 50% of the curvature of the Lesser Caucasus fold-and-thrust belt formed after the Eocene and probably before the Late Miocene (Meijers et al., 2015a, b). This agrees well with the existence of an Early-Middle Miocene phase of

deformation, as argued in this paper. The analysis of published literature (including the available geological maps) and preliminary field data point to a few large structures which might have driven to a large extent the thermal evolution of the study area. For example, the complex fault system northeast of the town of Dilijan in the hanging wall of the Sevan-Akera suture (Fig. 2) separates the two groups of FT ages and must have played a part in the differential exhumation of the samples analyzed in this paper. Such complex structure comprises (i) a large East–West-trending, south-dipping reverse fault and (ii) a NE–SW-trending transpressional fault system separating not reset Late Cretaceous FT ages to the SE from Miocene ages to the NW. This fault array does not seem to continue into the footwall block, whose western part is also characterized by Miocene cooling ages (a few Ma older than those in the hanging wall). The fact that Miocene cooling ages occur both in the hanging wall and footwall of the Sevan-Akera main thrust fault suggests that the overall exhumation pattern in this portion of the Lesser Caucasus cannot be simply the result of the reactivation of that thrust, although such a reactivation could account for the offset of ca. 5 Ma in the AFT cooling ages between hanging wall and footwall blocks (~12 Ma vs. ~17 Ma, respectively) across the thrust.

The Lesser Caucasus low-temperature thermochronologic evolution during the Neogene—with particular reference to Miocene cooling—can be framed within a broader context by comparing it to the results of recent thermochronometric studies in adjacent regions of eastern Anatolia, as shown in Fig. 7 and discussed below. Exhumation of Cretaceous–Eocene granitoids along the Black Sea coast in the eastern Pontides region also occurred in the Miocene (Albino et al., 2014), mirroring the age of maximum tectonic coupling between the Eurasia and Arabia plates along the 2400 km long Bitlis-Zagros suture zone, some 200 km to the south (Okay et al., 2010). Long-range deformation focused along the Black Sea coast at the boundary between polydeformed continental lithosphere and pristine—and rheologically stronger—oceanic lithosphere of the Eastern Black Sea. Conversely, apatite FT ages across the Anatolian Plateau are consistently Paleogene (with a cluster of ages in the Middle-Late Eocene). Over this wide region, Eocene cooling was the last thermochronologically significant result of the contractional deformation related to the closure of the Izmir-Ankara-Erzincan ocean and the ensuing collision between the Sakarya and Anatolide-Tauride terranes. The memory of this continental accretion has been retained by the AFT thermochronometer because exhumation during the creation of the Anatolian Plateau was insufficient to unroof a new apatite partial annealing zone (Cavazza et al., 2017, 2018). Stress from the Bitlis collision zone was transmitted heterogeneously in the region of the Lesser Caucasus. The Adjara-Trialeti zone of western Georgia was structurally affected but exhumation was insufficient to expose a new apatite PAZ (Albino et al., 2014). This paper documents that in other areas of the Lesser Caucasus exhumation (i) was large enough to expose to the surface a new PAZ, (ii) was coeval with the Arabia-Eurasia collision, and (iii) focused along preexisting structural discontinuities, i.e. segments of the Amasia-Sevan-Akera suture zone.

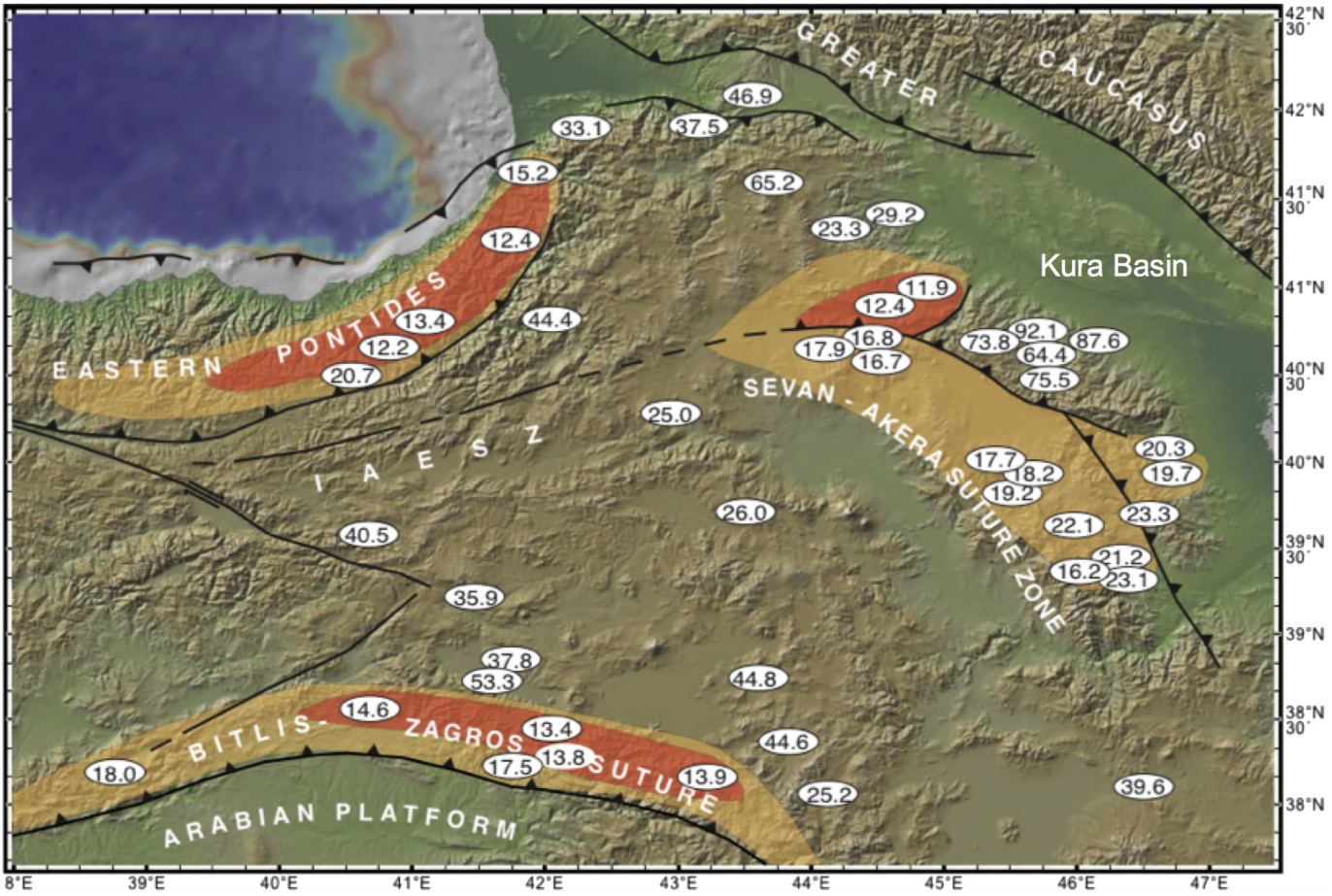

Figure 7. Areal distribution of apatite fission-track ages in eastern Anatolia and Transcaucasia. Dark orange: ages <15 Ma; light orange: ages 22–15 Ma. All other FT ages are older than 22 Ma. IAESZ: Izmir-Ankara-Erzincan suture zone. Sources of data: Okay et al. (2010); Albino et al. (2014); Cavazza et al. (2017, 2018); this study.

From a wider, more interpretative perspective, the integration of present-day crustal dynamics and low-temperature thermochronometric data available for Asia Minor— as summarized in Fig. 7— provides a comparison between short- and long-term deformation patterns for the entire eastern Anatolian-Transcaucasian region and has some bearing on the timing of the overall westward "tectonic escape" of Anatolia. Present-day GPS velocity patterns indicate that most of the Arabia-Eurasia convergence is now accommodated by the westward movement of the Anatolian plate (Fig. 8) which has largely decoupled the Anatolian hinterland from the Bitlis collision zone. GPS velocities (and seismicity) are now very low in the Eastern Pontides and the Lesser Caucasus, where contractional exhumation was rapid during the Early-Middle Miocene (Albino et al., 2014; Meijers et al., 2015a, b; Cavazza et al., 2017, 2018; this paper). Two successive stages of Neogene deformation of the hinterland of the Arabia-Eurasia collision zone can thus be inferred (Fig. 9). (1) During the Early Miocene, continental deformation was concentrated along the Arabia-Eurasia (Bitlis) collision zone but tectonic stresses were transmitted over a wider area and focused along the coast of the eastern Black Sea and in the Lesser Caucasus, inducing significant shortening and exhumation. The Black Sea (quasi)oceanic lithosphere is rheologically stronger than the polydeformed Anatolian continental lithosphere to the south and therefore acted as a "backstop" resisting deformation and deviating the impinging continental lithosphere (McClusky et al., 2000). Other small areas along kinematic block boundaries may have been affected. From this viewpoint, it should be noted that the set of Miocene AFT ages in NW Armenia presented by Albino et al. (2014) and compiled in this paper was yielded by samples close to the boundary between kinematic blocks proposed by Reilinger et al. (2006) based on the analysis of GPS motion vectors. (2) Since late Middle Miocene time the activation of the North and Eastern Anatolian Fault systems and the connate westward translation of Anatolia have triggered a new tectonic regime: most of the Arabia-Eurasia convergence is now being accommodated by the westward motion of Anatolia whereas the eastern Pontides are mechanically decoupled from the Bitlis collision zone. Stress has continued to be transferred efficiently toward the Caucasian region, as shown by the structural inversion of the Kura-Rioni Basin (Alania et al., 2017) and the rapid exhumation of the Greater Caucasus in the Pliocene (Avdeev and Niemi, 2011). It could be argued that the transition between the two successive deformation stages may have occurred any time between the Middle Miocene and the present, but independent stratigraphic and structural data clearly indicate that the North Anatolian Fault system was activated in the mid-Miocene (for a review, see Şengör et al., 2005). Thus, the transition between shortening-dominated and strike-slip-dominated deformation occurred most likely in the Middle Miocene, shortly after maximum mechanical coupling between Arabia and Eurasia.

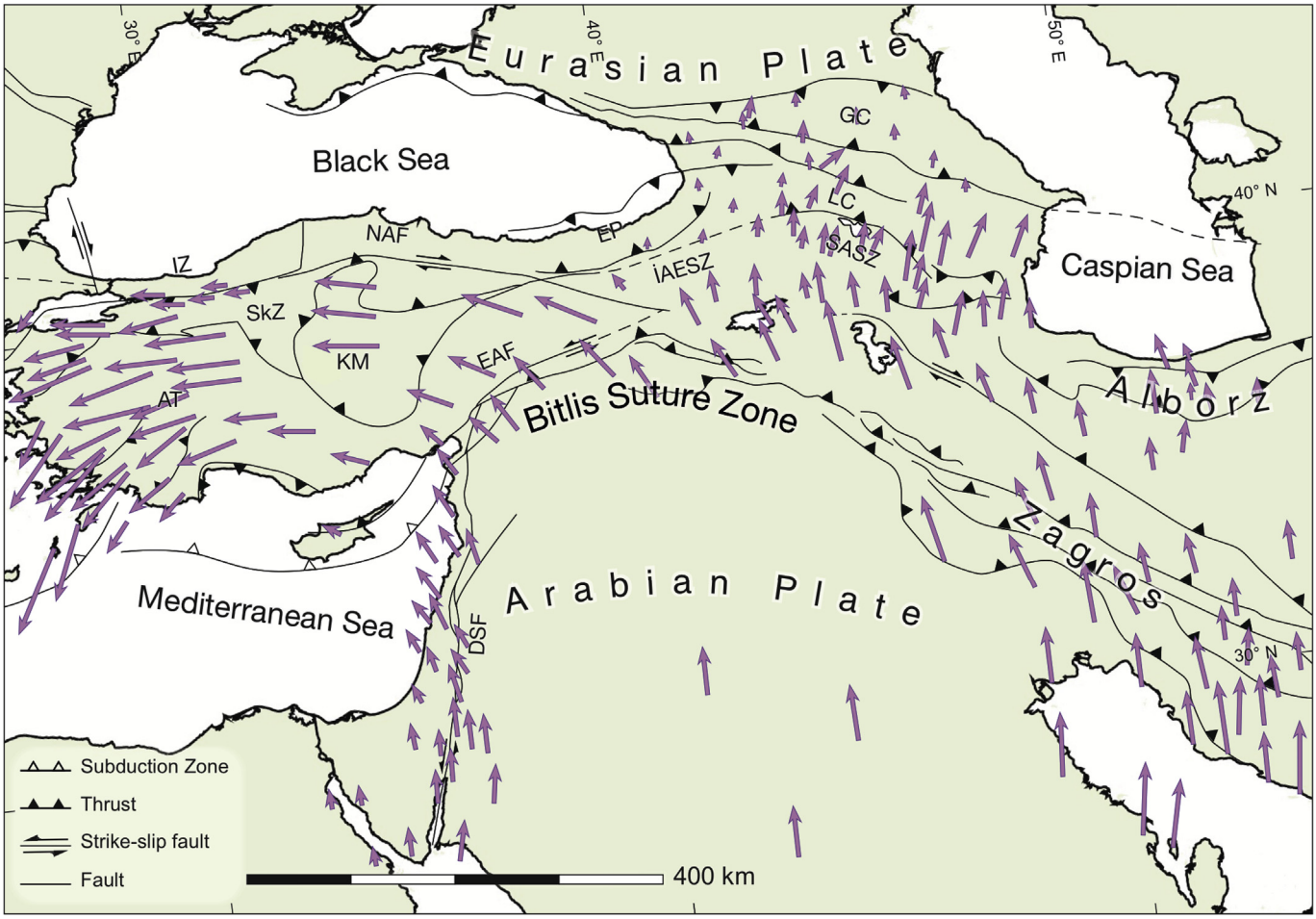

Figure 8. GPS motion vectors in the Middle East (from Le Pichon and Kreemer, 2010). AT: Anatolide-Tauride block; DSF: Dead Sea Fault; EAF: East Anatolian Fault system; EP: Eastern Pontides; GC: Greater Caucasus; İAESZ: İzmir-Ankara-Erzincan suture zone; IZ: Istanbul Zone; KM: Kirsehir Massif; LC: Lesser Caucasus; NAF: North Anatolian Fault system; SASZ: Sevan-Akera suture zone; SkZ: Sakarya Zone.

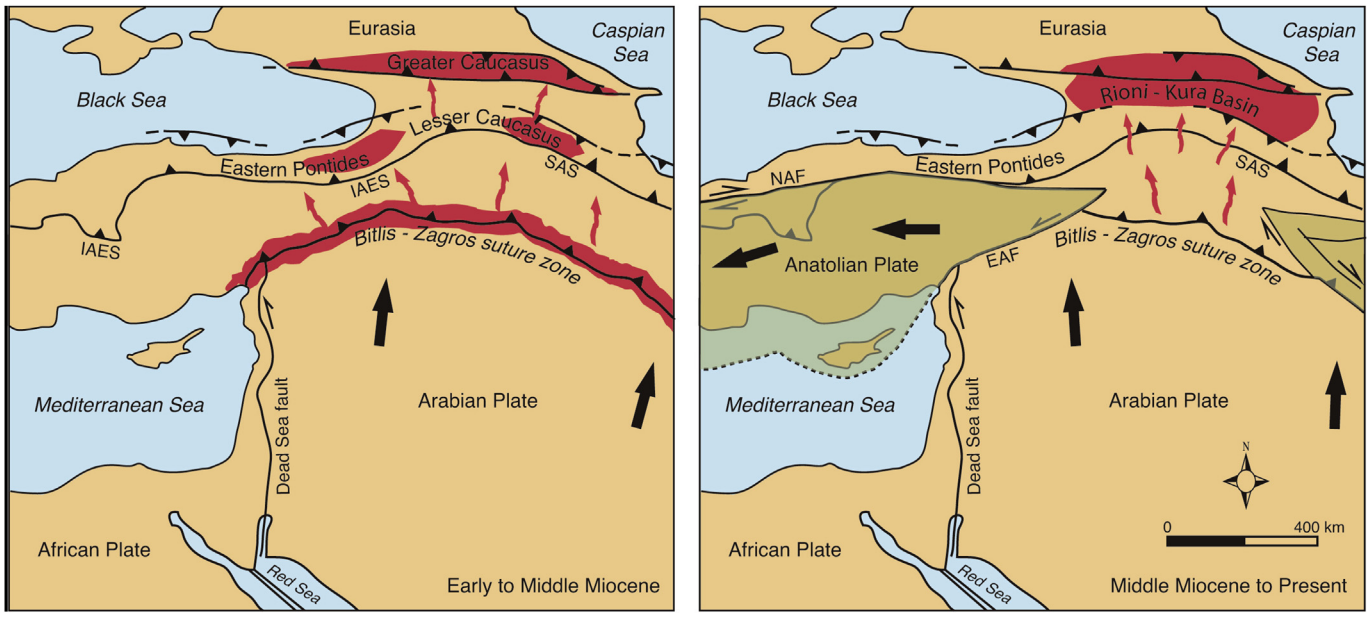

Figure 9. Non-palinspastic reconstructions of Neogene deformation patterns in the Eurasian hinterland of the Bitlis-Zagros collision zone. The development and westward movement of the Anatolian Plate has decoupled to a large extent the collision zone from its hinterland. Red arrows show stress transmissal away from the collision zone. Dark red indicates areas of focused deformation/exhumation, as determined by fission-track analysis. The plate velocity field (black arrows) is only schematically shown.

Shortening is still ongoing in the Greater Caucasus and the Rioni-Kura Basin, but most of the hinterland of the Bitlis collision zone has been since then dominated by strike-slip tectonics.

6. Conclusions

This paper presents the first comprehensive low-temperature thermochronologic survey of the entire Lesser Caucasus. The integration of the thermochronometric data presented here and pre-existing stratigraphic-structural data generates constraints relevant to the overall geological evolution of the Lesser Caucasus and the Middle East as a whole. AFT analyses point to a coherent Early-Middle Miocene episode of cooling/exhumation along the Paleocene–Eocene ASA suture zone which was likely reactivated by far-field stresses during Miocene collision along the Arabia-Eurasia collision zone, some 250 km to the south. The Miocene AFT ages along the ASA suture zone correlate well with other evidences of coeval cooling to the west. A compilation of all available fission-track data for the Bitlis-Zagros collision zone, the eastern Anatolian Plateau, the eastern Pontides, the Adjara-Trialeti fold-and-thrust belt of western Georgia, and the Lesser Caucasus shows clearly that Miocene cooling/exhumation occurred not only along the Arabia-Eurasia collision front but affected also selected portions of the Eurasian hinterland, i.e. the easternmost Pontides and the Lesser Caucasus. Conversely, cooling at temperatures below the apatite partial annealing zone in the Anatolian Plateau occurred in the Paleogene (with a cluster of ages in the Middle-Late Eocene), coevally with the development of the İzmir-Ankara-Erzincan suture (e.g. Okay and Tüysüz, 1999). This indicates that the entire region occupied nowadays by the plateau was largely bypassed by the tectonic stresses related to the collision and never underwent significant exhumation.

Despite the vastity of the area compared to the relatively small number of samples and the widespread cover of mostly Plio-Quaternary volcanics characterizing eastern Anatolia and Transcaucasia, this study shows that significant Miocene-age deformation occurred only at the margins of the Anatolian-Iranian Plateau. Synchronous deformation at the opposing ends of the Anatolian continental plateau reproduces the results of recent studies that identified deformation at the northern margin of the Tibetan Plateau, synchronous with the early stage of India-Asia collision (e.g. Clark et al., 2010).

Acknowledgments

Stimulating field discussions with S. Adamia (Inst. of Geophysics, Tbilisi), V. Alania (Tbilisi State Univ.), O. Enukidze (Tbilisi State Univ.), N. Imamverdiyev (Baku State Univ.), R. Melkonyan (Acad. of Sciences, Yerevan), A.I. Okay (Istanbul Technical Univ.) and N. Sadradze (Inst. of Geology, Tbilisi) were instrumental for introducing the senior author to the geology of the Lesser Caucasus. Comments by Y. Rolland and an anonymous reviewer greatly improved an earlier version of this manuscript. Funding for this research was provided by MIUR (Italian Ministry of University and Research) PRIN funds and the University of Bologna RFO funds. Thanks to the National Academy of Sciences (Yerevan) for logistical support.

References

Abdullayev, R.N., 1963. The Mesozoic Volcanism of the North-Eastern Part of the Lesser Caucasus. Publishing House, Academy of Sciences of Azerb. SSR, Baku, p. 228 (in Russian).

Adamia, S., Belov, A., Kekelia, M., Shavishvili, I., 1987. Paleozoic tectonic development of the Caucasus and Turkey (Geotraverse C). In: Flugel, H.W., Sassi, F.P., Grecula, P. (Eds.), Pre-Variscan and Variscan Events in the Alpine–Mediterranean Mountain Belts. Mineralia Slovaca, Alfa Bratislava, pp. 23–50.

Adamia, S., Zakariadze, G., Chkhotua, T., Sadradze, N., Tsereteli, N., Chabukian, A., Gventsadze, A., 2011. Geology of the Caucasus: a review. Turkish Journal of Earth Sciences 20, 489–544.

Agard, P., Omrani, J., Jolivet, L., Mouthereau, F., 2005. Convergence history across Zagros (Iran): constraints from collisional and earlier deformation. International Journal of Earth Sciences 94, 401–419.

Alania, V.M., Chabukiani, A.O., Chagelishvili, R.L., Enukidze, O.V., Gogrichiani, K.O., Razmadze, A.N., Tsereteli, N.S., 2017. Growth structures, piggy-back basins and growth strata of the Georgian part of the Kura foreland fold–thrust belt:

implications for Late Alpine kinematic evolution. Geological Society London Special Publications 428, 171–185.
Alavi, M., 1994. Tectonics of the Zagros orogenic belt of Iran: new data and interpretations. Tectonophysics 229, 211–238.
Albino, I., Cavazza, W., Zattin, M., Okay, A.I., Adamia, S., Sadradze, N., 2014. Far-field tectonic effects of the Arabia-Eurasia collision and the inception of the North Anatolian Fault system. Geological Magazine 151, 372–379.
Allen, M.B., Armstrong, H.A., 2008. Arabia–Eurasia collision and the forcing of mid-Cenozoic global cooling. Palaeogeography, Palaeoclimatology, Palaeoecology 265, 52–58.
Alsharhan, A.S., Nairn, A.E.M., 1997. Sedimentary Basins and Petroleum Geology of the Middle East. Elsevier, p. 843.
Arakelyan, R.A., 1964. The Paleozoic-Mesozoic. In: The Geology of the Armenian SSR: Stratigraphy. Publishing House of the AS of the Armenian SSR, Yerevan, pp. 21–163 (in Russian).
Aslanyan, A.T., Satian, M.A., 1977. On the geological features of Transcaucasian ophiolitic zones. Izvestia Academy Science Armenian SSR Nauki o Zemle 4–5, 13–26 (in Russian).
Avagyan, A., Sosson, M., Philip, H., Karakhanian, A., Rolland, Y., Melkonyan, R., Rebaï, S., Davtyan, V., 2005. Neogene to Quaternary stress field evolution in Lesser Caucasus and adjacent regions using fault kinematics analysis and volcanic cluster data. Geodinamica Acta 18, 401–416.
Avdeev, B., Niemi, N.A., 2011. Rapid Pliocene exhumation of the Central Greater Caucasus constrained by low-temperature thermochronometry. Tectonics 30 (2), TC2009. https://doi.org/10.1029/2010TC002808.
Barrier, E., Vrielynck, B., 2008. Paleotectonic Maps of the Middle East – Tectono-Sedimentary-Palinspastic Maps from Late Norian to Pliocene. Commission for the Geological Map of the World.
Berberian, M., King, G.C.P., 1981. Towards a paleogeography and tectonic evolution of Iran. Canadian Journal of Earth Sciences 18, 210–265.
Cavazza, W., Albino, I., Zattin, M., Galoyan, G., Imamverdiyev, N., Melkonyan, R., 2017. Thermochronometric evidence for Miocene tectonic reactivation of the Sevan-Akera suture zone (Lesser Caucasus): a far-field tectonic effect of the Arabia-Eurasia collision?. In: Sosson, M., Stephenson, R.A., Adamia, S.A. (Eds.), Tectonic Evolution of the Eastern Black Sea and Caucasus, vol. 428. Geological Society of London Special Publication, pp. 187–198. https://doi.org/10.1144/SP428.4.
Cavazza, W., Cattò, S., Zattin, M., Okay, A.I., Reiners, P., 2018. Thermochronology of the Miocene Arabia-Eurasia collision zone of southeastern Turkey. Geosphere 14 (5), 2277–2293.
Cavazza, W., Roure, F., Spakman, Stampfli, G.M., Ziegler, P.A., 2004. In: The TRANSMED Atlas: The Mediterranean Region from Crust to Mantle. Springer-Verlag, Heidelberg, p. 141. +CD-ROM.
Clark, M.K., Farley, K.A., Zheng, D., Wang, Z., Duvall, A.R., 2010. Early Cenozoic faulting of the northern Tibetan Plateau margin from apatite (U–Th)/He ages. Earth and Planetary Science Letters 296, 78–88.
Cloetingh, S.A.P.L., Wortel, M.J.R., Vlaar, N.J., 1982. State of Stress at Passive Margins and Initiation of Subduction Zones: Tectonic Processes: Model Investigations of Margin Environmental and Tectonic Processes, vol. 34. AAPG Memoir, pp. 717–723.
Cloetingh, S., Wortel, R., Vlaar, N.J., 1989. On the initiation of subduction zones. Pure and Applied Geophysics 129, 7–25.
Cloetingh, S.A.P.L., Ziegler, P.A., Beekman, F., Andriessen, P.A.M., Matenco, L., Bada, G., Garcia-Castellanos, D., Hardebol, N., Dèzes, P., Sokoutis, D., 2005. Lithospheric memory, state of stress and rheology: neotectonic controls on Europe's intraplate continental topography. Quaternary Science Reviews 24, 241–304.
Cowgill, E., Forte, A.M., Niemi, N., Avdeev, B., Tye, A., Trexler, C., Godoladze, T., 2016. Relict basin closure and crustal shortening budgets during continental collision: an example from Caucasus sediment provenance. Tectonics 35, 2918–2947.
Danelian, T., Zambetakis-Lekkas, A., Galoyan, G., Sosson, M., Asatryan, G., Hubert, B., Grigoryan, A., 2014. Reconstructing upper Cretaceous (Cenomanian) paleoenvironments in Armenia based on Radiolaria and benthic Foraminifera; implications for the geodynamic evolution of the Tethyan realm in the Lesser Caucasus. Palaeogeography, Palaeoclimatology, Palaeoecology 413, 123–132.
Dewey, J.F., Hempton, M.R., Kidd, W.S.F., Saroglu, F., Şengör, A.M.C., 1986. Shortening of continental lithosphere: the neotectonics of Eastern Anatolia—a young collision zone. Geological Society London Special Publication 19, 1–36.
Donelick, R.A., O'Sullivan, P.B., Ketcham, R.A., 2005. Apatite fission-track analysis. Reviews in Mineralogy and Geochemistry 58, 49–94.
Ehlers, T.A., Chaudhri, T., Kumar, S., Fuller, C.W., Willett, S.D., Ketcham, R.A., Brandon, M.T., Belton, D.X., Kohn, B.P., Gleadow, A.J., Dunai, T.J., 2005. Computational tools for low-temperature thermochronometer interpretation. Reviews in Mineralogy and Geochemistry 58, 589–622.
Galoyan, G.L., 2008. Petrologic, Geochemical and Geochronological Studies of the Ophiolites of the Lesser Caucasus (Armenia). PhD thesis, University of Nice-Sophia Antipolis, p. 287 (in French).
Galoyan, G.L., Melkonyan, R.L., Atayan, L.S., Chung, S.-L., Khorenyan, R.H., Lee, Y.-H., Amiraghyan, S.V., 2018. On the Petrology and Geochemistry of Jurassic Magmatics of the Somkheti Segment of Somkheto-Karabagh Tectonic Zone (Northern Armenia).
Galoyan, G.L., Melkonyan, R.L., Chung, S.-L., Khorenyan, R.H., Atayan, L.S., Hung, C.-H., Amiraghyan, S.V., 2013. On the petrology and geochemistry of Jurassic Island-arc magmatics of the Karabagh segment of the Somkheto–Karabagh terrain. In: Proceedings of the NAS of the Republic of Armenia, Earth Sciences, vol. 66, pp. 3–22 (in Russian).
Galoyan, G., Rolland, Y., Sosson, M., Corsini, M., Billo, S., Verati, C., Melkonyan, R., 2009. Geology, geochemistry and $^{40}Ar/^{39}Ar$ dating of Sevan ophiolites (Lesser Caucasus, Armenia): evidence for Jurassic back-arc opening and hot spot event between the South Armenian Block and Eurasia. Journal of Asian Earth Sciences 34, 135–153.
Gleadow, A.J.W., Fitzgerald, P.G., 1987. Uplift history and structure of the Transantarctic Mountains: new evidence from fission track dating of basement apatites in the Dry Valleys area, southern Victoria Land. Earth and Planetary Science Letters 82, 1–14.
Hall, R., 1976. Ophiolite emplacement and the evolution of the Taurus suture zone, southeastern Turkey. Geological Society of America Bulletin 87, 1078–1088.
Hässig, M., Rolland, Y., Duretz, T., Sosson, M., 2016a. Obduction triggered by regional heating during plate reorganization. Terra Nova 28 (1), 76–82.
Hässig, M., Duretz, T., Rolland, Y., Sosson, M., 2016b. Obduction of old oceanic lithosphere due to reheating and plate reorganization: insights from numerical modelling and the NE Anatolia-Lesser Caucasus case example. Journal of Geodynamics 96, 35–49.
Hässig, M., Rolland, Y., Sahakyan, L., Sosson, M., Galoyan, G., Avagyan, A.,, Müller, C., 2015b. Multi-stage metamorphism in the south Armenian block during the late Jurassic to early Cretaceous: tectonics over south-dipping subduction of northern branch of Neotethys. Journal of Asian Earth Sciences 102, 4–23.
Hässig, M., Rolland, Y., Sosson, M., 2015a. From seafloor spreading to obduction: Jurassic-Cretaceous evolution of the northern branch of the Neotethys in the Northeastern Anatolian and Lesser Caucasus regions. Geological Society London Special Publications 428. SP428-10.
Hässig, M., Rolland, Y., Sosson, M., Galoyan, G., Muller, C., Avagyan, A., Sahakyan, L., 2013a. New structural and petrological data on the Amasia ophiolites (NW Sevan–Akera suture zone, Lesser Caucasus). Insights for a large-scale obduction in Armenia and NE Turkey. Tectonophysics 588, 135–153.
Hässig, M., Rolland, Y., Sosson, M., Galoyan, G., Sahakyan, L., Topuz, G., Müller, C., 2013b. Linking the NE Anatolian and Lesser Caucasus ophiolites: evidence for large-scale obduction of oceanic crust and implications for the formation of the Lesser Caucasus-Pontides Arc. Geodinamica Acta 26, 311–330.
Hurford, A.J., Green, P.F., 1983. The zeta age calibration of fission-track dating. Chemical Geology 41, 285–317.
Jassim, S.Z., Goff, J.C. (Eds.), 2006. Geology of Iraq. DOLIN sro, distributed by Geological Society of London, p. 341.
Jolivet, L., Faccenna, C., 2000. Mediterranean extension and the Africa-Eurasia collision. Tectonics 19, 1095–1106.
Jolivet, L., Huchon, P., Rangin, C., 1989. Tectonic setting of Western Pacific marginal basins. Tectonophysics 160, 23–47.
Ketcham, R.A., 2005. Forward and inverse modeling of low-temperature thermochronometry data. Reviews in Mineralogy and Geochemistry 58, 275–314.
Ketcham, R.A., Carter, A., Donelick, R.A., Barbarand, J., Hurford, A.J., 2007. Improved modeling of fission-track annealing in apatite. American Mineralogist 92, 799–810.
Ketcham, R.A., Donelick, R.A., Carlson, W.D., 1999. Variability of apatite fission-track annealing kinetics: III. Extrapolation to geological time scales. American Mineralogist 84, 1235–1255.
Khain, V.E., 1994. Geology of northern Eurasia (Ex-USSR). Second Part: Phanerozoic Fold Belts and Young Platforms. Gebrüder Borntraeger, Berlin, p. 404.
Knipper, A.L., 1975. The oceanic crust in the structure of the Alpine folded belt (south Europe, western part of Asia and Cuba). Transactions 267. Moscow 'Nauka' (in Russian).
Knipper, A.L., Khain, E.V., 1980. Structural position of ophiolites of the Caucasus. Ofioliti Special Issue, vol. 2, pp. 297–314.
Le Pichon, X., Kreemer, C., 2010. The Miocene-to-present kinematic evolution of the eastern Mediterranean and Middle East and its implications for dynamics. Annual Review of Earth and Planetary Sciences 38, 323–351.
McClusky, S., et al., 2000. Global Positioning System constraints on plate kinematics and dynamics in the eastern Mediterranean and Caucasus. Journal of Geophysical Research 105, 5695–5719.
Meijers, M.J., Smith, B., Kirscher, U., Mensink, M., Sosson, M., Rolland, Y., Müller, C., 2015a. A paleolatitude reconstruction of the south Armenian block (Lesser Caucasus) for the late Cretaceous: constraints on the Tethyan realm. Tectonophysics 644, 197–219.
Meijers, M.J., Smith, B., Pastor-Galán, D., Degenaar, R., Sadradze, N., Adamia, S., Sahakyan, L., Avagyan, A., Sosson, M., Rolland, Y., Langereis, C.G., Müller, C., 2015b. Progressive orocline formation in the eastern Pontides-Lesser Caucasus. Geological Society London Special Publications 428. SP428-8.
Melkonyan, R.L., 1989. Petrology and Ore-Bearing Capacity of the Mesozoic Island-Arc Granitoid Formations of the Lesser Caucasus: Summary of Sciences Thesis, Moscow, p. 50 (in Russian).
Melkonyan, R.L., Chung, S.-L., Ghukasyan, R.K., Galoyan, G.L., Khorenyan, R.H., Atayan, L.S., 2016. The geology and isotope dating of the Tsav intrusive complex (Southern Armenia, Kapan terrain). In: Proceed. NASRA, Earth Sciences, vol. 69, pp. 3–23 (in Russian).
Ministry of Geology of the USSR, 1952a. Geological Map of the USSR, 1:200,000 scale, sheet K-38-XXVII.
Ministry of Geology of the USSR, 1952b. Geological Map of the USSR, 1:200,000 scale, sheet K-38-XXXIII.
Ministry of Geology of the USSR, 1952c. Geological Map of the USSR, 1:200,000 scale, sheet K-38-XXXV.

Ministry of Geology of the USSR, 1952d. Geological Map of the USSR, 1:200,000 scale, sheet J-38-V.
Ministry of Geology of the USSR, 1971. Geological Map of the USSR, 1:200,000 scale, sheet J-38-XI.
Moritz, R., Rezeau, H., Ovtcharova, M., Tayan, R., Melkonyan, R., Hovakimyan, S., Ramazanov, V., Selby, D., Ulianov, A., Chiaradia, M., Putlitz, B., 2016. Long-lived, stationary magmatism and pulsed porphyry systems during Tethyan subduction to post-collision evolution in the southernmost Lesser Caucasus, Armenia and Nakhitchevan. Gondwana Research 37, 465–503.
Okay, A.I., Tüysüz, O., 1999. Tethyan sutures of the northern Turkey. In: Durand, B., Jolivet, L., Horvát, F., Sérrane, M. (Eds.), The Mediterranean Basins: Tertiary Extension within the Alpine Orogen, vol. 156. Geological Society of London Special Publication, pp. 475–515.
Okay, A.I., Zattin, M., Cavazza, W., 2010. Apatite fission-track data for the Miocene Arabia-Eurasia collision. Geology 38, 35–38.
Reilinger, R., McClusky, S., Vernant, P., Lawrence, S., Ergintav, S., Cakmak, R., Ozener, H., Kadirov, F., Guliev, I., Stepanyan, R., Nadariya, M., Hahubia, G., Mahmoud, S., Sakr, K., Arrajehi, A., Paradissis, D., Al-Aydrus, A., Prilepin, M., Guseva, T., Evren, E., Dmitrotsa, A., Filikov, S.V., Gomez, F., Al-Ghazzi, R., Karam, G., 2006. GPS constraints on continental deformation in the Africa-Arabia-Eurasia continental collision zone and implications for the dynamics of plate interactions. Journal of Geophysical Research 111 (B5), B05411.
Rezeau, H., Moritz, R., Wotzlaw, J.F., Tayan, R., Melkonyan, R., Ulianov, A., Stern, R.A., 2016. Temporal and genetic link between incremental pluton assembly and pulsed porphyry Cu-Mo formation in accretionary orogens. Geology 44 (8), 627–630.
Rezeau, H., Moritz, R., Leuthold, J., Hovakimyan, S., Tayan, R., Chiaradia, M., 2017. 30 Myr of Cenozoic magmatism along the Tethyan margin during Arabia-Eurasia accretionary orogenesis (Meghri-Ordubad pluton, southernmost Lesser Caucasus). Lithos 288, 108–124.
Ricou, L.E., Dercourt, J., Geyssant, J., Grandjacquet, C., Lepvrier, C., Biju-Duval, B., 1986. Geological constraints on the Alpine evolution of the Mediterranean Tethys. Tectonophysics 23, 83–122.
Robertson, A.H.F., 2002. Overview of the genesis and emplacement of Mesozoic ophiolites in the eastern Mediterranean Tethyan region. Lithos 65, 1–67.
Robertson, A.H.F., Parlak, O., Rizaoğlu, T., Ünlügenç, Ü., İnan, N., Tasli, K., Ustaömer, T., 2007. Tectonic evolution of the south Tethyan ocean: evidence from the eastern Taurus Mountains (Elazığ region, SE Turkey). In: Ries, A.C., Butler, R.W.H., Graham, R.H. (Eds.), Deformation of Continental Crust. Geological Society, London, Special Publication, pp. 231–270, 272.
Rolland, Y., Billo, S., Corsini, M., Sosson, M., Galoyan, G., 2009a. Blueschists of the Amassia-Stepanavan suture zone (Armenia): linking Tethys subduction history from E-Turkey to W-Iran. International Journal of Earth Sciences. https://doi.org/10.1007/s00531-007-0286-8.
Rolland, Y., Galoyan, G., Sosson, M., Melkonyan, R., Avagyan, A., 2010. The Armenian ophiolite: insights for Jurassic back-arc formation, lower Cretaceous hot spot magmatism and upper Cretaceous obduction over the south Armenian block. In: Stephenson, R.A., Starostenko, V., Bergerat, F. (Eds.), Sedimentary Basins Tectonics from the Black Sea to the Arabian Platform, vol. 340. Geological Society, London, Special Publications, pp. 353–382.
Rolland, Y., Hässig, M., Bosch, D., Meijers, M.J.M., Sosson, M., Bruguier, O., Sadradze, N., 2016. A review of the plate convergence history of the East Anatolia-Transcaucasus region during the Variscan: insights from the Georgian basement and its connection to the Eastern Pontides. Journal of Geodynamics 96, 131–145.
Rolland, Y., Perincek, D., Kaymakci, N., Sosson, M., Barrier, E., Avagyan, A., 2012. Evidence for ~ 80–75 Ma subduction jump during Anatolide-Tauride-Armenian block accretion and ~ 48 Ma Arabia-Eurasia collision in Lesser Caucasus-East Anatolia. Journal of Geodynamics 56, 76–85.
Rolland, Y., Sosson, M., Adamia, S., Sadradze, N., 2011. Prolonged Variscan to Alpine history of an active Eurasian margin (Georgia, Armenia) revealed by $^{40}Ar/^{39}Ar$ dating. Gondwana Research 20, 798–815.
Şengör, A.M.C., Tüysüz, O., İmren, C., Sakınç, M., Eyidoğan, H., Görür, N., Le Pichon, X., Rangin, C., 2005. The North Anatolian fault: a new look. Annual Review of Earth and Planetary Sciences 33, 37–112.
Sokolov, S.D., 1977. The Olistostromes and Ophiolitic Nappes of the Lesser Caucasus Izdatelstvo 'Nauka', Moscow (in Russian).
Sosson, M., Rolland, Y., Müller, C., Danelian, T., Melkonyan, R., Kekelia, S., Adamia, S., Babazadeh, V., Kangarli, T., Avagyan, A., Galoyan, G., Mosar, J., 2010. Subductions, obduction and collision in the Lesser Caucasus (Armenia, Azerbaijan, Georgia), New Insights. Geological Society of London Special Publication 340, 329–352.
Sosson, M., Stephenson, R., Sheremet, Y., Rolland, Y., Adamia, S., Melkonian, R., Kangarli, T., Yegorova, T., Avagyan Galoyan, G., Danelian, T., Hassig, M., Meijers, M., Müller, C., Sahakyan, L., Sadradze, N., Alania, V., Enukidze, O., Mosar, 2016. The eastern Black Sea-Caucasus region during the Cretaceous: new evidence to constrain its tectonic evolution. Comptes Rendus Geoscience 348, 23–32.
Stampfli, G., Borel, G., Cavazza, W., Mosar, J., Ziegler, P.A. (Eds.), 2001. The Paleotectonic Atlas of the PeriTethyan Domain. CD-ROM. European Geophysical Society.
Stampfli, G.M., Hochard, C., 2009. Plate tectonics of the Alpine realm. Geological Society London Special Publication 327, 89–111.
Topuz, G., Candan, O., Zack, T., Yılmaz, A., 2017. East Anatolian plateau constructed over a continental basement: No evidence for the east Anatolian accretionary complex. Geology 45, 791–794.
Yılmaz, E., Duran, O., 1997. Stratigraphic lexicon for the authochthonous and allochthonous units of Southeast Anatolia. Publication No. 31. Türkiye Petrolleri A.O. Research Center, p. 460 (in Turkish).
Yılmaz, Y., 1993. New evidence and model on the evolution of the southeast Anatolian orogen. Geological Society of America Bulletin 105, 251–271.
Ziegler, P.A., 1993. Plate-moving mechanisms: their relative importance. Journal of the Geological Society 150, 927–940.
Ziegler, P.A., Cloetingh, S., Van Wees, J.-D., 1995. Dynamics of intra-plate compressional deformation: the Alpine foreland and other examples. Tectonophysics 252, 7–59.
Ziegler, P.A., Van Wees, J.-D., Cloetingh, S., 1998. Mechanical controls on collision-related compressional intraplate deformation. Tectonophysics 300, 103–129.
Ziegler, P.A., Bertotti, G., Cloetingh, S.A.P.L., 2002. Dynamic processes controlling foreland development - the role of mechanical (de) coupling of orogenic wedges and forelands. Stephan Mueller Special Publication Series 1, 17–56.
Zoback, M.L., 1992. First-and second-order patterns of stress in the lithosphere: the World Stress Map Project. Journal of Geophysical Research Solid Earth 97, 11703–11728.
Zonenshein, L.P., Kuzmin, M.I., Natapov, L.M., 1990. Geology of the USSR: a plate-tectonic synthesis. American Geophysical Union Geodynamics Series 21, 242.